The Behavior of a Stiff Clay behind Embedded Integral Abutments

Ming Xu [1], Alan G. Bloodworth [2] and Chris R.I. Clayton [3]

Abstract

Integral bridges can significantly reduce maintenance and repair costs compared with conventional bridges. However, uncertainties have arisen in the design as the soil experiences temperature-induced cyclic loading behind the abutments. This paper presents the results from an experimental programme on the behavior of Atherfield Clay, a stiff clay from the UK, behind embedded integral abutments. Specimens were subjected to the stress paths and levels of cyclic straining that a typical embedded integral abutment might impose on its retained soil. The results show that daily and annual temperature changes can cause significant horizontal stress variations behind such abutments. However, no build-up in lateral earth pressure with successive cycles was observed for this typical stiff clay, and the stress-strain behavior and stiffness behavior were not influenced by continued cycling. The implications of the results for integral abutment design are discussed.

CE Database subject headings: Abutments; Clays; Stress strain relations; Young's modulus; Cyclic loads; Triaxial tests.

1. Engineer, Mott MacDonald, Croydon, CR9 2UL, UK. (Formerly Research Fellow, School of Civil Engineering and the Environment, University of Southampton). Email: Ming.Xu@mottmac.com

2. Lecturer, School of Civil Engineering and the Environment, University of Southampton, SO17 1BJ, UK. Email: agb2@soton.ac.uk

3. Professor, School of Civil Engineering and the Environment, University of Southampton, SO17 1BJ, UK. Email: c.clayton@soton.ac.uk

The Behavior of a Stiff Clay behind Embedded Integral Abutments

Ming Xu, Alan G. Bloodworth and Chris R.I. Clayton

INTRODUCTION

A traditional road bridge comprises a superstructure supported by abutments at each end and possibly also by intermediate piers. To accommodate the superstructure length change caused by daily and annual temperature variation, the superstructure is isolated from the abutments by means of expansion joints and bearings.

Since the 1970's, the disadvantages of this approach of using expansion joints and bearings have become apparent to bridge engineers. A survey of 200 concrete bridges in the UK (Wallbank 1989) showed that when deck movement joints leak, the resulting penetration of de-icing salts from the highway on to the sub-structure components is the most serious source of damage to these components, and that corrosion and immobilization of the movement joints and bearings also occurrs. Furthermore, these joints and bearings are expensive to purchase, install and maintain, and have a short life compared to the design life of the bridge as a whole (Biddle et al. 1997). Replacement operations are highly disruptive to traffic flow and very expensive.

Integral bridges, which have no bearings or expansion joints, were seen as a solution to the above problems. Integral bridges are becoming increasingly popular around the world, especially in the United States, Sweden and the United Kingdom (Burke 1990; Hambly 1997). For example, the UK design standard BD 57/95, *Design for Durability* (Highways Agency 1995), required that the integral option be considered for new bridges under 60 m span and with less than 30° skew.

Integral abutments can be categorized into three types: shallow abutments (bank seats), full height frame abutments on spread footings, and full height embedded abutments. Shallow abutments and frame abutments normally retain granular backfill. Embedded abutments (diaphragm or bored pile walls) are usually constructed in *in-situ* clayey ground, followed by bridge deck installation, and then by open excavation between abutments to form the underpass. Compared with the other two abutment types, embedded abutments (Figure 1a) require less land-take and introduce less disturbance, making them particularly attractive in urban areas. The construction of embedded integral abutment bridges has become common in the UK during the past two decades (e.g. Barker and Carder 2000; Place et al. 2005), and is likely to become more attractive in other parts of the world, considering the increasing demand for construction of new roads or upgrading of old roads within expanding cities.

Overconsolidated stiff clay is an important ground condition in some countries, *e.g.* the UK (Gaba et al. 2003). Design and construction of embedded

integral abutments in stiff clay is frequently required (Card and Carder 1993; Biddle et al. 1997; Way and Yandzio 1997; Barker and Carder 2000; Place et al. 2005).

However, with a fixed connection between the superstructure and the abutments, the abutments are forced to move towards or away from the soil they retain as daily and annual temperature variation causes deck length change. As a consequence, the retained soil is subjected to horizontal cyclic loading. There is uncertainty amongst designers about the extent to which the properties of soils, *e.g.* stiffness, may change when subjected to this type of loading, and consequently also about the ultimate magnitude of the lateral earth pressure behind the abutments.

Limited laboratory experiments on integral abutments have been conducted in the past decade, mainly centrifuge tests (Springman et al. 1996; Ng et al. 1998; Tapper and Lehane 2004) and 1-g model tests (England et al. 2000; Cosgrove and Lehane 2003). Field monitoring has also been carried out on integral abutments (*e.g.* Broms and Ingleson 1971; Hoppe and Gomez 1996; Darley et al. 1996; Barker and Carder 2000). Most work has only considered granular materials. Only Barker and Carder (2000) reported field monitoring of an integral bridge with abutments embedded in stiff clay. However, lateral pressure was only measured for reinforced soil near the surface. No measurement was made in the deeper stiff clay. In addition, this investigation lasted for only about 2 years after construction, and was complicated by the creep and shrinkage of the concrete during and after construction. Engineers

therefore face significant uncertainties in the design of abutments embedded in stiff clay (*e.g.* Way and Yandzio 1997).

The aim of this paper is to present a fundamental approach to determining the mechanical behavior of stiff clay behind an embedded integral abutment wall, with the aim of improving guidance for designers.

LABORATORY STRESS PATH TESTING

In general, the stress-strain behavior of soil is dependent on the stress path followed (Lambe 1967; Lade and Duncan 1976). Appropriate deformation characteristics may only be obtained if the appropriate stress path is followed. Similarly, for a given deformation or strain level, realistic stress changes will not be estimated unless appropriate stress paths are followed. To obtain a thorough understanding of the stress-strain relationship for stiff clay in the integral bridge situation, geotechnical laboratory stress path testing has been carried out.

The prototype bridge abutment under consideration (Figure 1a) has a retained height of 8 m, with an embedded length of 12 m. The range of deck expanding lengths considered was from 30 m to 90 m. A key soil element was considered at half the retained height, *i.e.* at a depth of 4 m below the top of the bridge deck.

Total Stress Path

The effect of the wall movement is to cause a horizontal strain in the soil, leading to a change in horizontal stress. The total vertical stress is constant and fixed by the weight of overburden (for a wall assumed to be smooth). For simplicity, the intermediate stress is ignored and the tests were conducted in the triaxial apparatus (Lambe and Marr 1979). The total stress path in the soil is represented in Figure 1b.

Cyclic Radial Strain Range

Both field monitoring (Barker and Carder 2000) and numerical modelling (Lehane 1999) have demonstrated that the retained soil can provide only limited restraint to deck expansion or contraction. Assuming equal movement at both ends of the deck, a coefficient of thermal expansion of reinforced concrete $\alpha = 12 \times 10^{-6}/^{o}C$ and an annual effective bridge temperature (EBT) range of $43^{o}C$ in the London area (Highways Agency 2001), the total annual abutment displacement at the end of a 60 m concrete bridge deck is approximately 16 mm.

Finite element analysis was carried out (Xu 2005) to investigate the cyclic lateral strain behind an abutment. It was found that the change of soil stiffness has only a marginal effect on the cyclic lateral strain magnitude, in contrast to the dominant influences of the geometry of the wall and the top displacement. For the abutment in Figure 1a at the end of a 60 m long deck, the cyclic lateral strain in the key soil element is about 0.08%.

This strain level is comparable to that calculated using a simplified method (Bolton and Powrie 1988), which considers a rigid wall (total length h) rotating around its toe by a top displacement δ, for which the lateral strain in the retained soil can be approximated as δ/h. An embedded integral abutment is more likely to rotate around a pivot some distance above the toe, as observed in the FE analysis and in the centrifuge testing (Springman et al. 1996).

Testing Equipment

An automated triaxial cyclic loading system was developed based on Bishop and Wesley hydraulic triaxial apparatus. Control software was designed capable of performing radial strain-controlled cyclic loading tests on 100 mm diameter specimens along the desired stress path (Figure 1b) over long periods of time, with measured total vertical stress varying by less than 0.3 kPa from the desired constant value (Xu 2005). Pressures and displacements were driven by GDS advanced controllers. To avoid potential errors introduced by external strain measurement (Baldi et al. 1988), strains were measured locally over the mid third height of the specimen using submersible LVDTs (Cuccovillo and Coop 1997), with a resolution of about 0.00015 mm and with electronic noise minimized. Deviator stress was measured by an internal submersible load cell, while pore water pressure was measured locally at the mid height using a flushable mid-plane probe with a high-air-entry stone (Sodha 1974).

Materials Tested

The stiff clay used in the testing was Atherfield Clay, originating from a depth of about 15~17 m at the site of a cut-and-cover tunnel at Ashford, Kent, UK (Richards et al. 2006). Atherfield Clay is a stiff to very stiff, closely fissured clay with a chocolate brown colour, about 4.5 m thick at this location and with a plasticity index of 20-30%. It was deposited approximately during the geological period of Lower Cretaceous. Electron micrographs demonstrate a very dense and anisotropic arrangement of platy particles (Figure 2).

The micro-structure of natural soils has significant influence on their behavior (e.g. Leroueil and Vaughan 1990). The disturbance to the micro-structure of surrounding soils during *in situ* installation of diaphragm or bored pile walls depends on details of construction and ground conditions, but is believed to be only significant within a very limited distance from the wall, *e.g.* a maximum of 0.5 m in stiff clay (Richards et al. 2006). "Undisturbed" samples were therefore used.

Two undisturbed Atherfield Clay specimens (AC2 and AC3) were subjected to cyclic stress path testing. Another specimen (AC1) was tested under monotonic shearing. AC1 and AC2 were obtained by wireline drilling, while AC3 was obtained by block sampling. Both sampling methods are believed to be capable of obtaining high quality samples of overconsolidated clay (Clayton et al. 1995). To check the inevitable disturbance during the sampling process, the initial mean effective stress measured in the triaxial apparatus was compared with the estimated *in situ* mean effective stress, and good

agreement was found for all specimens. This suggests that the overall level of disturbance was low.

A knife was initially used to cut the samples into cylinders that were slightly larger than the required specimen size. For the block sample, care was taken to maintain the orientation of the specimen as *in situ*. A soil lathe was used to trim the specimen surface, and a two-part metal mould was used to trim the ends of the specimens to ensure a right cylindrical geometry.

In situ clays in the UK are usually saturated, since the water table is normally high (*e.g.* about 1~2 m below ground level at the sampling site) and the pore size is sufficiently small to sustain high suction without air entry occurring. The specimens were therefore tested in a saturated condition in this research. The specimens were saturated in the triaxial cell by increasing the cell pressure in steps with the back drainage line closed until a satisfactory B value of at least 0.95 was achieved.

Initial Stress State

Although the *in situ* earth pressure coefficient K_o in heavily overconsolidated clay is usually high, especially at shallow depth (Skempton 1961), the installation of diaphragm or piled walls will usually significantly reduce the horizontal earth pressure, such that the earth pressure coefficient K can drop to around 1 (Clayton and Milititsky 1983; Tedd et al. 1984). Excavation in front of the wall will further reduce the horizontal earth pressure, although this

effect is more difficult to predict, since it depends on the detail of the construction sequence.

To reflect these uncertainties, different initial stress states were chosen for specimens AC2 and AC3. Specimen AC2 was first swelled isotropically to an effective stress of about 80 kPa, which replicated the stress condition inside the key soil element after the installation of the diaphragm wall in stiff clay. Then the effect of excavation in front of the wall was simulated by reducing the radial stress under undrained conditions with a constant total vertical stress until a radial strain of 0.05% was reached. Cyclic loading was started from this stress state (σ_h'= 74 kPa, σ_v'= 88 kPa). For specimen AC3, a well-propped wall was assumed, so only the effect of wall installation was incorporated, giving an initially isotropic stress state of σ_h'= σ_v'= 76 kPa.

Testing Procedure

Atherfield Clay is a heavily overconsolidated stiff clay with a very low permeability (c_v= 2.2 m²/year), while drainage is not installed behind embedded abutments due to the *in situ* construction. The key soil element is therefore likely to experience lateral cyclic loading under undrained conditions, especially for daily cycles.

Undrained radial strain-controlled cyclic loading was applied on both specimens (AC2 and AC3) along the total stress path shown in Figure 1b with a rate of 2% external axial strain per day. This rate was slow enough for pore water pressure to equilibrate inside the soil, as well as following the desired

stress path closely. For each specimen, the smallest cyclic radial strain ranges were applied first, to minimise the risk of destructuring. At a particular radial strain range, cycling was continued until it became evident that the soil stress-strain relationship was no longer changing with cycling, *i.e.*, the soil had entered a "resilient" state. The cyclic radial strain range was then increased to a larger magnitude. AC2 was tested under cyclic radial strain ranges of 0.04% (5 cycles) and 0.075% (3 cycles). AC3 was tested under cyclic radial strain ranges of 0.025% (6 cycles), 0.05% (6 cycles), 0.1% (4 cycles) and 0.15% (1 cycle).

At the end of each compression and extension radial strain excursion, the radial strain was held constant for a rest period to reduce the effects of stress relaxation (creep) to an acceptable level. This avoids continued stress relaxation influencing the stiffness behavior in the next excursion, especially at small strain levels, leading to incorrect measurements of stiffness (Clayton and Heymann 2001). In this research, the deviator stress relaxation rate was allowed to reduce to less than 1% of the initial deviator stress increase rate before the next radial strain excursion was commenced.

Following undrained cyclic loading, AC2 was sheared in radial extension to failure. To investigate the drained behaviour of the key soil element, as well as stiffness at different effective stress levels, and soil strength, AC3 was further tested in three stages. First, it was subjected to a single drained radial strain-controlled cycle. Then the specimen was consolidated isotropically to $p_o{'} = 115$ kPa, at which an undrained radial strain-controlled cycle was carried

12

out.   Finally the specimen was consolidated to $p_o{}'$ = 230 kPa and then sheared, but under a constant cell pressure.

RESULTS AND DISCUSSION

Undrained Stress-strain Behavior

Both specimens, AC2 and AC3, exhibited a very similar pattern of deviator stress-radial strain behavior over a range of different cyclic radial strain ranges.   Typical deviator stress-radial strain curves for AC2 (0.075%) and AC3 (0.1%), as well as corresponding effective stress paths, are presented in Figure 3 and Figure 4 respectively.   Each radial strain excursion led to a change of deviator stress (and radial stress), which was reduced to some extent by stress relaxation during the following rest period.   During the first strain excursion at a particular radial strain level, the soil was slightly stiffer than in the previous excursion as the previous radial strain level was being exceeded.   However, in the subsequent strain excursions, such a pattern was not maintained, but instead the soil returned to follow the trend defined by the previous strain range, and the soil stress-strain relationship became identical and repeatable for each cycle.   The soil was thus deemed to have entered a "resilient" state. There was no perceptible accumulation of deviator stress with cycling.

The effective stress paths for specimens AC2 and AC3 did not follow a constant mean effective stress (p') line, which indicates a strong anisotropy in stiffness (Graham and Houlsby 1983) and will be discussed further later.

13

There was no sign of yielding. For specimen AC2, no obvious difference was found between each strain excursion, though there was a slight variation in the mid-plane pore water pressure. For specimen AC3, a small difference can be seen between the compression and extension effective stress paths, probably due to the stress paths crossing the isotropic line.

Shearing of AC1, AC2 and AC3 at different effective stress levels reveals an effective friction angle $\varphi' = 26^o$ and an effective cohesion $c' = 10$ kPa.

Undrained Stiffness Behavior

Previous researchers have been concerned that the stiffness of clay behind an integral abutment may change due to the temperature-induced cyclic loading, presenting a major uncertainty for design of the structure. In this research, the undrained stiffness of Atherfield Clay under cyclic loading has been examined extensively, especially at appropriate small strain levels.

As predicted, the axial strain was found to be overestimated by external measurement, compared with local measurement using LVDTs. The error was much more significant during the initial strain excursions, but it reduced with increasing number of cycles, probably due to the removal of the bedding errors under cyclic loading.

For convenient comparison with other research on soil stiffness, all stiffnesses are quantified in terms of secant Young's modulus. A number of factors that might influence the soil stiffness have been investigated.

Influence of direction of radial strain excursion

Figure 5 plots a typical pair of compression and extension stiffness-radial strain curves from one cycle for specimens AC2 and AC3. The stiffness of the soil is highly nonlinear. For AC2, no obvious difference was observed in either the value of the maximum stiffness at very small strains or the rate of degradation of stiffness between the two curves. For AC3, the stiffness at very small strains is the same in compression and extension, but between approximately 0.005% and 0.1% radial strain the curves diverge slightly, probably reflecting the small difference between the compressive and extensive effective stress paths (Figure 4).

Influence of continued cycling

Comparison between typical stiffness-strain curves from different cycles under the same cyclic strain range is made in Figure 6. It is clear that cyclic loading did not change the soil stiffness behavior.

Influence of previous cyclic radial strain magnitude

Typical secant stiffness-radial strain curves under different cyclic radial strain ranges are compared in Figure 7. For AC2, no obvious difference was found. For AC3, despite the 300% increase in the strain range, the very small strain stiffness and the rate of degradation of stiffness with strain were almost unchanged, with only a very slight difference in stiffness near the end of each strain range. However, for practical purposes these curves may be considered identical.

Influence of initial stress states

During undrained cyclic loading, specimen AC2 always remained above the isotropic line, whereas specimen AC3 was tested crossing the isotropic line (Figures 3 and 4). Representative stiffness–strain curves for both specimens are compared in Figure 8. The stiffness has not been normalised, as the initial mean effective stresses (p'_o) for specimens AC2 (80 kPa) and AC3 (76 kPa) were similar. It can be seen that the two specimens exhibit almost identical stiffness characteristics.

Evidence for stiffness anisotropy

Figure 9 shows two curves of normalised horizontal stiffness against radial strain, compared with two curves of normalised vertical stiffness against axial strain. The normalised horizontal stiffness is seen to be higher than the normalised vertical stiffness. Further evidence of this stiffness anisotropy comes from the pore water pressure change against mean total stress change for specimens AC1 and AC3 during undrained shearing under constant cell pressure, and the volumetric strain against axial strain for AC3 during isotropic consolidation, which are shown in Figures 10 and 11 respectively, together with an idealized response of isotropic material superimposed (Graham and Houlsby 1983). These data suggest a strong anisotropy in stiffness, which is an inherent consequence of the microstructure of this stiff clay (Figure 2).

Comparison with sand stiffness behavior

The stiffness of Atherfield Clay is further compared with that of coarse sand (Figure 12), the behavior of which was also under investigation behind integral frame abutments (Xu 2005). In contrast to the high and continuingly increasing stiffness of sand, the stiffness of stiff clay was much lower and remained unchanged with cycling.

Micrographs (Figure 2) reveal that the Atherfield Clay particles have a sheet-like shape in general, with a very dense fabric of platy particles overlapping each other. Xu (2005) showed that the deformation of Atherfield Clay under loading is likely to be the result of recoverable platy-particle bending and compression; while for granular materials, the strain mainly involves sliding and rotation of granular particles.

Drained Stress-strain Behavior

To check whether drainage would lead to a build up of radial stress, drained cycling was carried out on specimen AC2. Because of the very slow loading rate (0.03% axial strain per day) required, only a single cycle was performed. The stress path in Figure 13 shows that even at this low rate of loading, full drainage was not achieved at the mid-plane of the specimen. After a full cycle with drainage both volumetric and radial strains were recoverable (Figure 13), and there was no obvious accumulation in radial stress.

Comparison with Field Monitoring on Propped Embedded Retaining Walls

Despite of the limited numbers of cycling compared with field conditions, the testing results described above strongly suggest that there would be no significant build-up of stresses in the long term. This is a result of the unchanged micro-structure of stiff clay during cycling, as indicated by the unchanged soil small strain stiffness (Hight et al. 1997). Further evidence emerges from previous long term field monitoring of the earth pressure behind propped retaining walls embedded in stiff clay.

Carder and Symons (1990) and Carder and Darley (1999) have reported field monitoring of a bored-pile wall embedded in London Clay and propped beneath the carriageway. As with an integral abutment bridge, seasonal temperature variation caused expansion and contraction of the prop slab. As a result, large fluctuations in the lateral earth pressures and pore water pressures were recorded near the retaining wall. However, after a period of 11 years, despite some minor redistribution of stress, there was no significant change in the magnitude or distribution of total lateral stresses.

Clark (2006) has reported the results of field monitoring during and after construction of a 12m wide double-propped retaining wall. The horizontal pressure measured in the Atherfield Clay at the mid retained height varied closely with daily and annual temperature variation, but no obvious build-up of lateral stress has been observed in the first 4 years after construction.

IMPLICATION FOR PRACTICE

Currently, no design standard or guidance has been published specifically on the earth pressure behind full-height embedded integral abutments in stiff clay. In practice, such abutments are sometimes treated as embedded retaining walls propped at the crest in the preliminary design, with active earth pressure assumed behind the wall (Gaba et al. 2003). The test results have confirmed that daily and annual temperature changes cause significant horizontal stress variations behind such abutments. The annual deck length change of a typical 60 m long concrete bridge can cause about 40 kPa variation in the horizontal earth pressure in the representative soil element 4 m below ground level (Figures 3 and 4). For an embedded abutment constructed in the winter, with equal horizontal and vertical pressures assumed after wall installation, such an increase implies a maximum total horizontal earth pressure of 1.5 times the total vertical pressure when the deck expands in the summer. This is much higher than active earth pressure.

This research has shown, however, that a build-up of horizontal earth pressure behind embedded integral abutments in clay over many daily or annual temperature cycles is not expected. This is markedly different from the observation on integral abutments backfilled by granular materials. Therefore, different design considerations should be given for the earth pressures behind integral abutments retaining *in situ* clay from those retaining granular backfill.

A more precise prediction of the magnitude and distribution of earth pressure behind embedded integral abutments and analysis of soil-structure interaction

19

requires numerical modelling, *e.g.* the finite element method. The soil stiffness used in the analysis is of paramount importance. Our research has demonstrated that the stiffness of stiff clay is strongly anisotropic, strain level dependent, and highly non-linear over the range of horizontal strains that can be expected behind typical embedded abutments. Evaluation of soil stiffness therefore requires horizontal loading coupled with small-strain stiffness measurement.

However, the stiffness behavior of the stiff clay examined in this research was found not to be obviously influenced by horizontal cyclic loading, over a wide range of strain levels. Therefore, pseudo-static numerical modelling can be used, with a monotonic displacement applied at the top of the wall. The constitutive model for the soil in such a model should adequately reflect the nonlinear variation of soil stiffness over the strain range from 0.001% to 0.1% where the stiffness decreases sharply. There are two alternative methods for achieving this:

(i)   Use a constitutive model that faithfully reflects the degradation of soil stiffness with strain, such as the non-linear soil model proposed by Jardine et al. (1986).

(ii)   Derive stiffness values for the soil related to particular horizontal strain levels that are appropriate for the geometry of the integral bridge and the temperature-induced movement range.

In this research a stiff clay was studied under saturated conditions. It is recognized that in other parts of the world there are different types of soils,

which could also be unsaturated (Fredlund and Rahardjo 1993). For simplicity the stiff clay specimens in this research were tested under triaxial conditions. Behind an abutment conditions may vary from plane strain (at the highway centreline) to approximately triaxial (at the edge of the abutment), but since plane strain testing is now extremely rare in geotechnical testing practice triaxial testing results are generally accepted as providing a reasonable estimate of behaviour.

This paper has concentrated on the effect of temperature-induced bridge deck length variation on the horizontal earth pressures behind embedded abutments of an integral bridge. There are other potential causes of deck length change, for example, in the case of a cast *in situ* reinforced concrete deck, thermal strain due to dissipation of the heat of hydration, drying shrinkage and creep under long-term loading. The magnitude of each of these effects depends on the composition of the concrete, the environmental conditions and the geometry of the member (Neville 1995). The construction sequence also has a major effect – for example if a concrete deck is cast in sections over a period of several days, the thermal strain will be much reduced, and if the deck is cast in isolation from the abutment walls, with the integral connection being made later, the effect of shrinkage will be reduced. In any case, each of these effects cause shortening the deck, moving the walls away from the soil, reducing the earth pressures. It is therefore conservative in the first instance to neglect these effects in the design.

ACKNOWLEDGEMENTS

NOTATION

The following symbols are used in this paper:

E_{uh}	=	undrained secant horizontal Young's modulus
E_{uv}	=	undrained secant vertical Young's modulus
K_0	=	coefficient of earth pressure *in situ*
p	=	mean total stress, $=(\sigma_v+2\sigma_h)/3$
p'	=	mean effective stress, $=(\sigma'_v+2\sigma'_h)/3$
p'_o	=	mean effective stress at the start of a stress excursion
q	=	deviator stress, $=\sigma_v-\sigma_h=\sigma'_v-\sigma'_h$
u	=	pore water pressure
ε_a	=	axial strain
ε_r	=	radial strain
ε_{vol}	=	volumetric strain
σ_v	=	vertical total stress
σ_h	=	horizontal total stress
σ'_v	=	vertical effective stress
σ'_h	=	horizontal effective stress

REFERENCES

Card, G.B. and Carder, D.R. (1993). *A literature review of the geotechnical aspects of integral bridge abutments*, TRL Project Report 52, Transport Research Laboratory, Crowthorne, Berks, UK.

Baldi, G., Hight, D.W., and Thomas, G.E. (1988). "A re-evaluation of conventional triaxial test methods." *Advanced Triaxial Testing of Soil and Rock*, ASTM STP 9777.

Barker, K.J. and Carder, D.R. (2000). *Performance of the two integral bridges forming the A62 Manchester road overbridge*, TRL Report 436, Transport Research Laboratory, Crowthorne, Berks, UK.

Biddle, A.R., Iles, D.C. and Yandzio, E.D. (1997). *Integral steel bridges: Design guidance*, SCI Publication P163, Steel Construction Institute, Ascot, Berks, UK.

Bolton, M.D. and Powrie, W. (1988). "Behaviour of diaphragm walls in clay prior to collapse." *Géotechnique*, 38(2), 167-189.

Broms, B.B. and Ingleson, I. (1971). "Earth pressure against the abutments of a rigid frame bridge." *Géotechnique*, 21(1), 15-28.

Burke, M.P. (1990). "Integral bridges." *Transportation Research Record*, No. 1275, 53-61.

Carder, D.R. and Darley, P. (1999). *The long term performance of embedded retaining walls*, TRL Report RP381, Transport Research Laboratory, Crowthorne, Berks, UK.

Carder, D.R. and Symons, I.F. (1990). *Long term performance of a propped retaining wall embedded in stiff clay*, TRL Report RP273, Transport Research Laboratory, Crowthorne, Berks, UK.

Clark, J. (2006). *Lateral stresses on in situ retaining walls in overconsolidated deposits*, PhD thesis, University of Southampton, UK.

Clayton, C.R.I. and Heymann, G. (2001). "The stiffness of geomaterials at very small strains." *Géotechnique*, 51(3), 245-256.

Clayton, C.R.I., Matthews, M.C. and Simons, N.E. (1995). *Site Investigation*, second edition, Blackwell Science, Oxford.

Clayton, C. R. I. and Milititsky, J. (1983). "Installation effects and the performance of bored piles in stiff clay." *Ground Engineering*, 16(2), 17-22.

Cosgrove, E.F. and Lehane, B.H. (2003). "Cyclic loading of loose backfill placed adjacent to integral bridge abutments." *International Journal of Physical Modelling in Geotechnics*, 3(3), 9-16.

Cuccovillo, T. and Coop, M. R. (1997). "The measurement of local axial strains in triaxial tests using LVDTs." *Géotechnique*, 47(1), 167–171.

Darley, P., Carder, D.R. and Alderman, G.H. (1996). *Seasonal thermal effects on the shallow abutment of an integral bridge in Glasgow*, TRL Report 178, Transport Research Laboratory, Crowthorne, Berks, UK.

England, G.L., Tsang, C.M. and Bush, D. (2000). *Integral Bridges - A Fundamental Approach to the Time Temperature Loading Problem*, Thomas Telford, London.

Fredlund, D.G. and Rahardjo, H.R. (1993). *Soil Mechanics for Unsaturated Soils*, John Wiley and Sons.

Gaba, A.R., Simpson, B., Powrie, W. and Beadman, D.R. (2003). *Embedded retaining walls—guidance for economic design*, CIRIA Report C580, Construction Industry Research and Information Association, London.

Graham, J. and Houlsby, G.T. (1983). "Elastic anisotropy of a natural clay." *Géotechnique*, 33(2), 165-180.

Hambly, E.C. (1997). "Integral bridges." *Proc. Inst. Civil Engnrs, Transport Engineering*, 123(1), 30-38.

Hight, D. W., Bennell, J. D., Chana, B., Davis, P. D., Jardine, R. J. and Porovic, E. (1997). "Wave velocity and stiffness measurements of the Crag and Lower London tertiaries at Sizewell." *Géotechnique*, 47(3), 451-474

Highways Agency (1995). *BD 57 Design for durability*, DMRB 1.3, HMSO, London.

Highway Agency (1996). *BA 42 The design of integral bridges*, DMRB 1.3, HMSO, London.

Highways Agency (2001). *BD 37 Loads for highway bridges*, DMRB 1.3, HMSO, London.

Hoppe, E. J. and Gomez, J.P. (1996). *Field study of an integral backwall bridge*, Virginia Transportation Research Council Final Report, Virginia Transportation Research Council, Charlottesville.

Jardine, R.J., Potts, D.M., Fourie, A.B. and Burland, J.B. (1986). "Studies of the influence of non-linear characteristics in soil-structure interaction." *Géotechnique*, 36(3), 377-396.

Lade, P.V. and Duncan, J.M. (1976). "Stress-path dependent behaviour of cohesionless soil." *Journal of the Geotechnical Engineering Division*, ASCE, 102(1), 51-68

Lambe, T.W. (1967). "Stress path method." *Journal of soil mechanics and foundation division*, ASCE, 93(SM6), 309-331.

Lambe, T.W. and Marr, W. A. (1979). "Stress path method: second edition." *Journal of geotechnical engineering*, ASCE, 105(GT6), 727–738.

Lehane, B.M. (1999). "Predicting the restraint provided to integral bridge deck expansion." *Proceeding of the Twelfth European Conference on Soil Mechanics and Geotechnical Engineering*, Amsterdam, Vol. 2, 797-802.

Leroueil, S. and Vaughan, P.R. (1990). "The general and congruent effects of structure in natural soils and weak rocks." *Géotechnique*, 40(3), 467–488.

Neville, A.M. (1995). *Properties of Concrete*, 4th edition, Longman, Harlow, UK.

Ng, C.W.W., Springman, S.M. and Norrish, A.R.M. (1998). "Centrifuge modelling of spread-base integral bridge abutments." *Journal of Geotechnical and Geoenvironmental Engineering*, ASCE, 124(5), 376-388.

Place, D., Farooq, I. and Carter, S. (2005). "A34 Chieveley/M4 junction 13 improvement: design." *Proceedings of the Institution of Civil Engineers, Bridge Engineering*, 158(1), 15-23.

Richards, D.J., Clark, J. and Powrie, W. (2006). "Installation effects of a bored pile wall in overconsolidated clay." *Géotechnique*, 56(6), 411-425.

Skempton, A.W. (1961). "Effective stress in soils, concrete and rocks." *Pore Pressure and Suction in Soils*, Butterworth, London.

Sodha, V. (1974). *The stability of embankment dam fills of plastic clays*. MPhil thesis, Imperial College, University of London.

Springman, S. M., Norrish, A. and Ng, C.W.W. (1996). *Cyclic loading of sand behind integral bridge abutments*, TRL Project Report 146, Transport Research Laboratory, Crowthorne, Berks, UK.

Tapper L. and Lehane B.M. (2004). "Lateral stress development on integral bridge abutments." *Proceedings of the Eighteenth Australasian*

Conference on Mechanics of Structures and Materials, Perth, Vol. 2, 1069-1076.

Tedd P., Chard B.M., Charles J.A. and Symons I.F. (1984). "Behavior of a propped embedded retaining wall in stiff clay at Bell Common Tunnel." *Géotechnique*, 34(4), 513-532.

Wallbank, J. (1989). *The performance of concrete in bridges: a survey of 200 highway bridges*, HMSO, London.

Way, J.A. and Yandzio, E. (1997). *Integral steel bridges: design of a single-span bridge - worked example*, SCI Publication P180, Steel Construction Institute, Ascot, Berks, UK.

Xu, M. (2005). *The behaviour of soil behind full-height integral abutments*, PhD thesis, University of Southampton, UK.
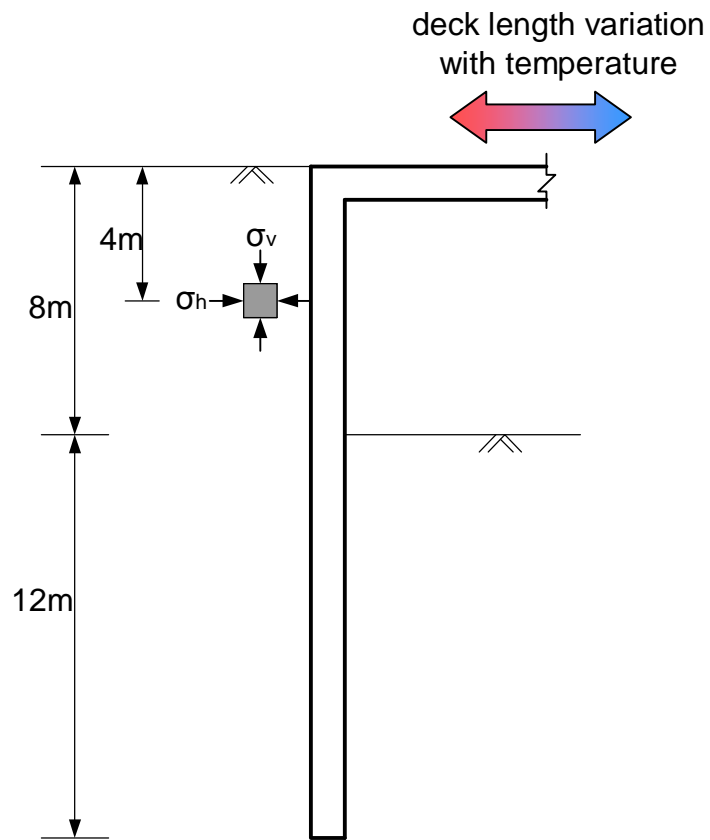
(a)
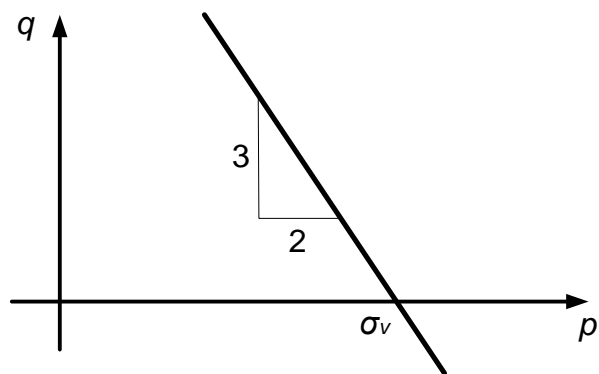
(b)

Figure 1. Location of the key soil element (a) and the total stress path (b)
for key soil element behind a smooth embedded integral abutment
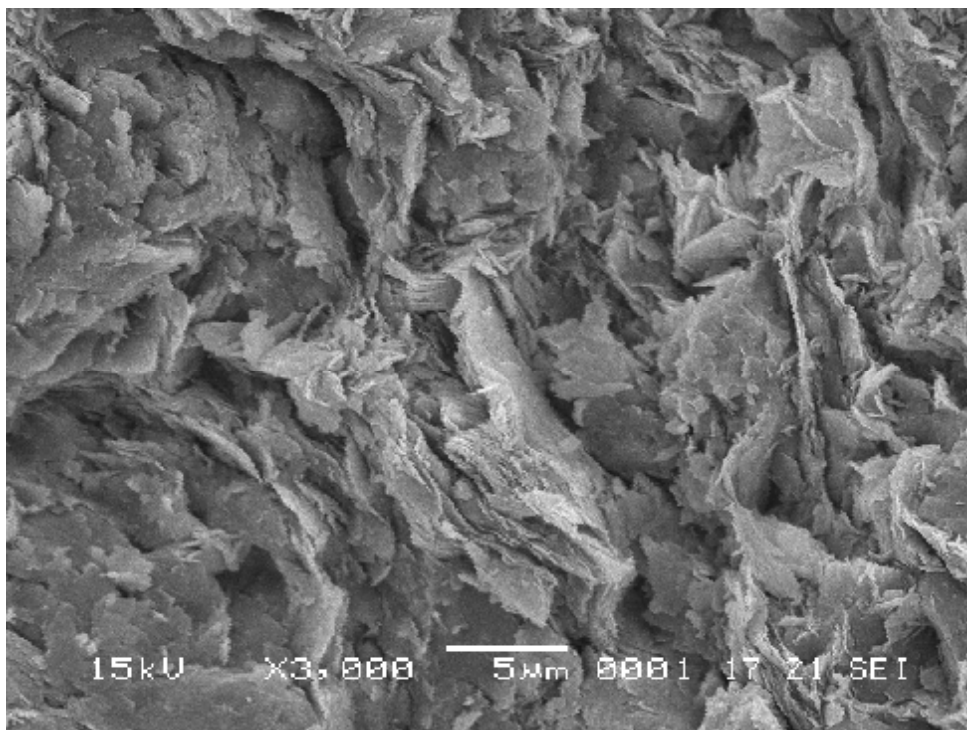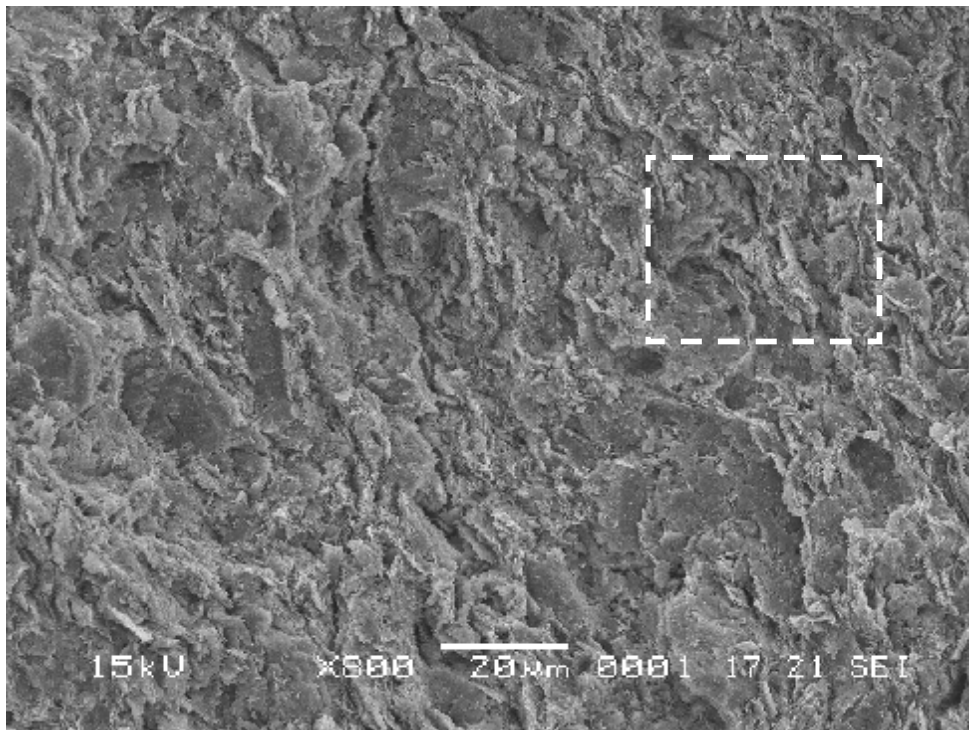
Figure 2. Scanning electron micrographs of Atherfield Clay
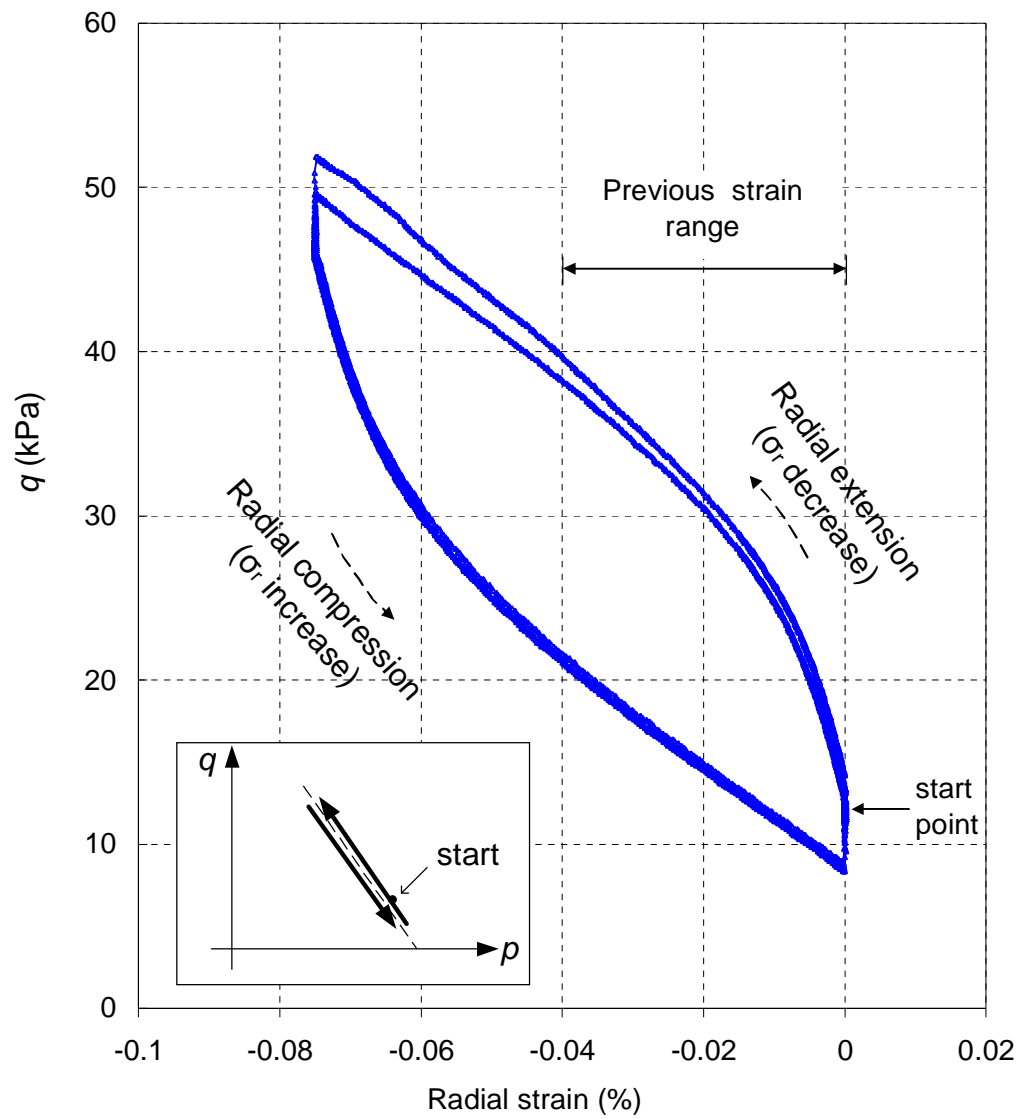
(a)
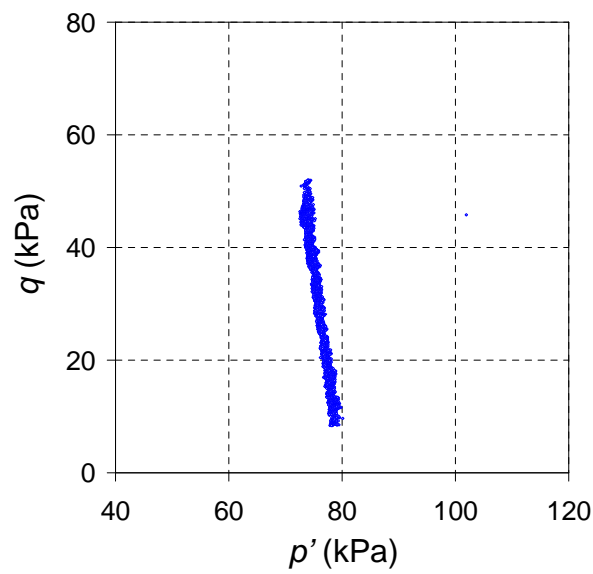
(b)

Figure 3. Deviator stress against radial strain (a), and effective stress paths (b), for specimen AC2 under an undrained cyclic radial strain range of 0.075% (3 cycles)
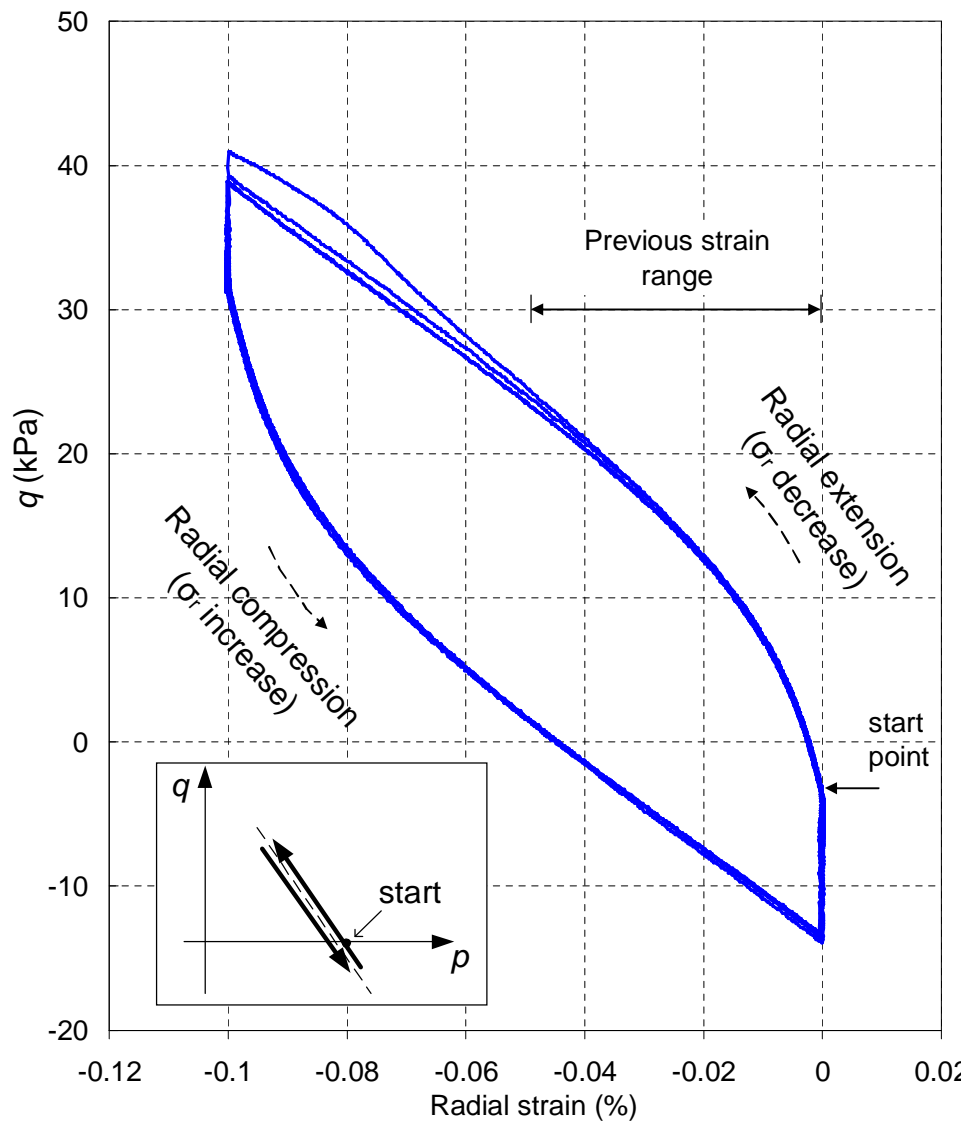
(a)
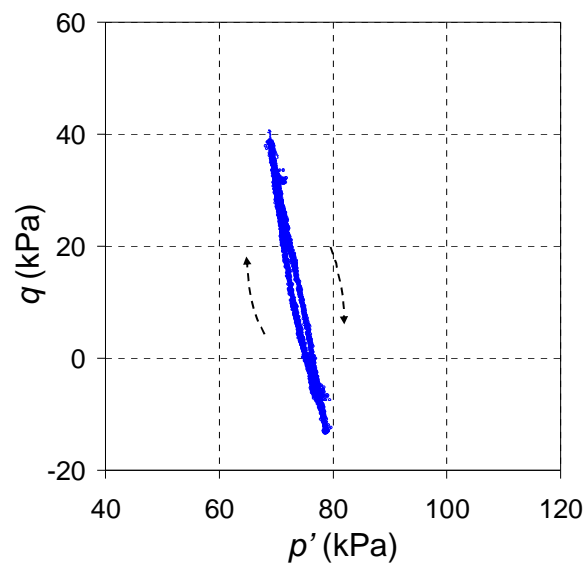
(b)

Figure 4. Deviator stress against radial strain (a), and effective stress paths (b), for specimen AC3 under an undrained cyclic radial strain of 0.1% (4 cycles)
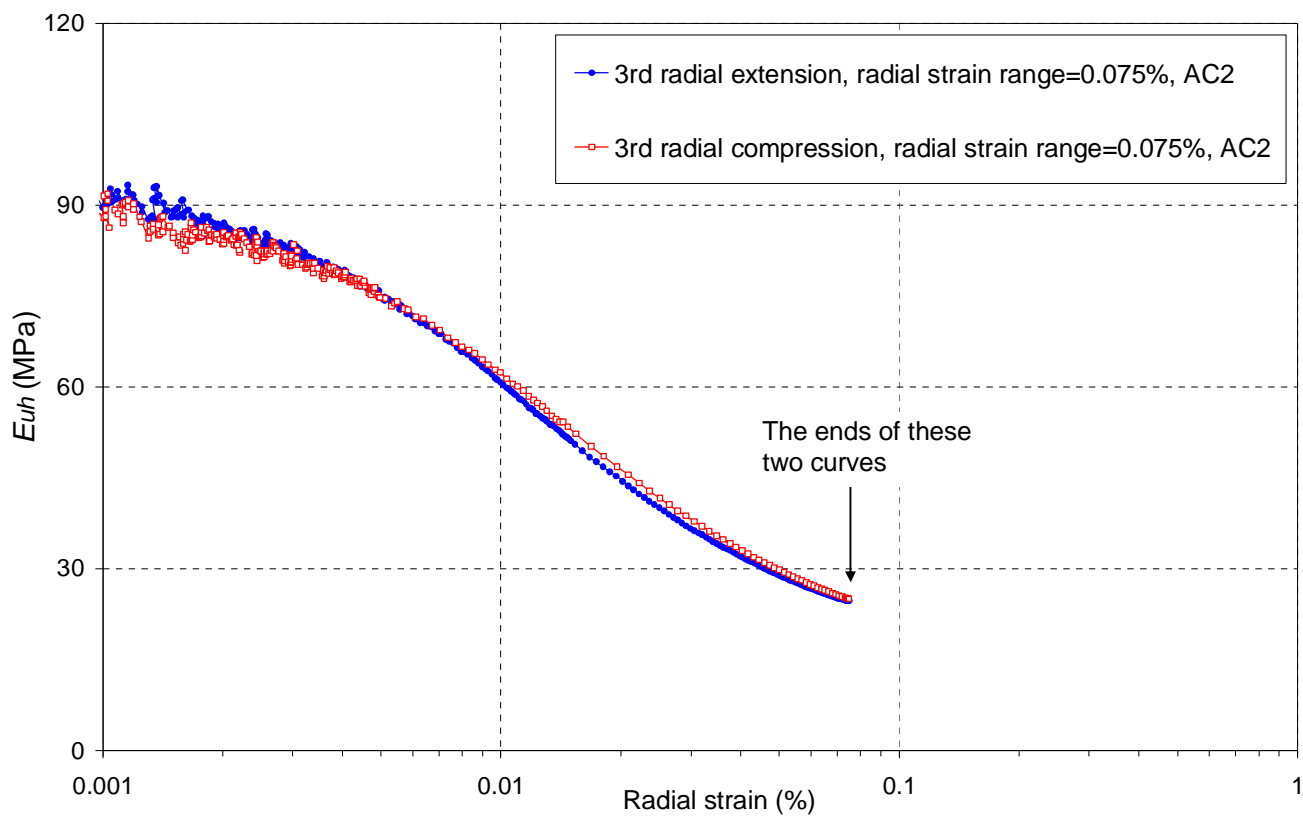
(a) Specimen AC2
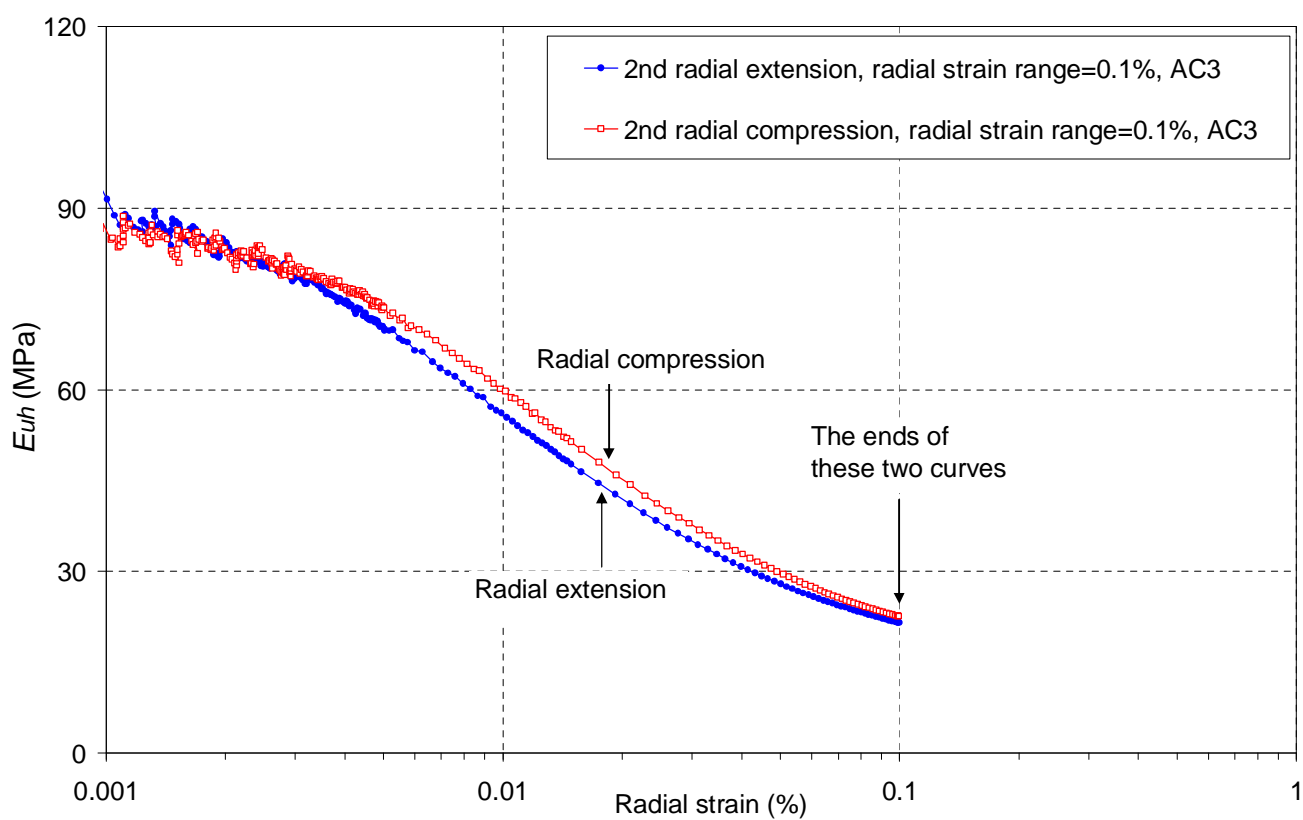
(b) Specimen AC3

Figure 5. Comparison of the secant undrained horizontal Young's modulus (E_{uh}) in radial compression and radial extension over one typical cycle
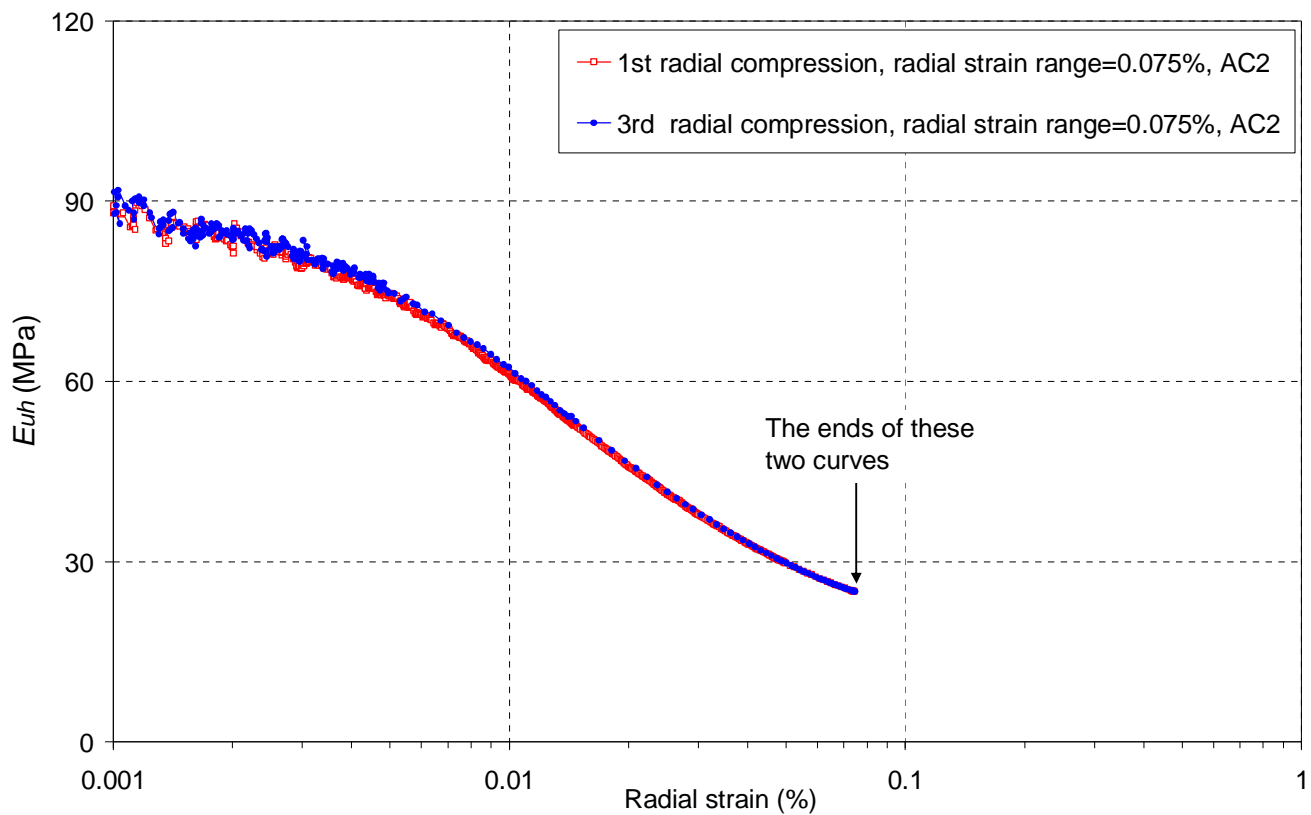
(a) Specimen AC2
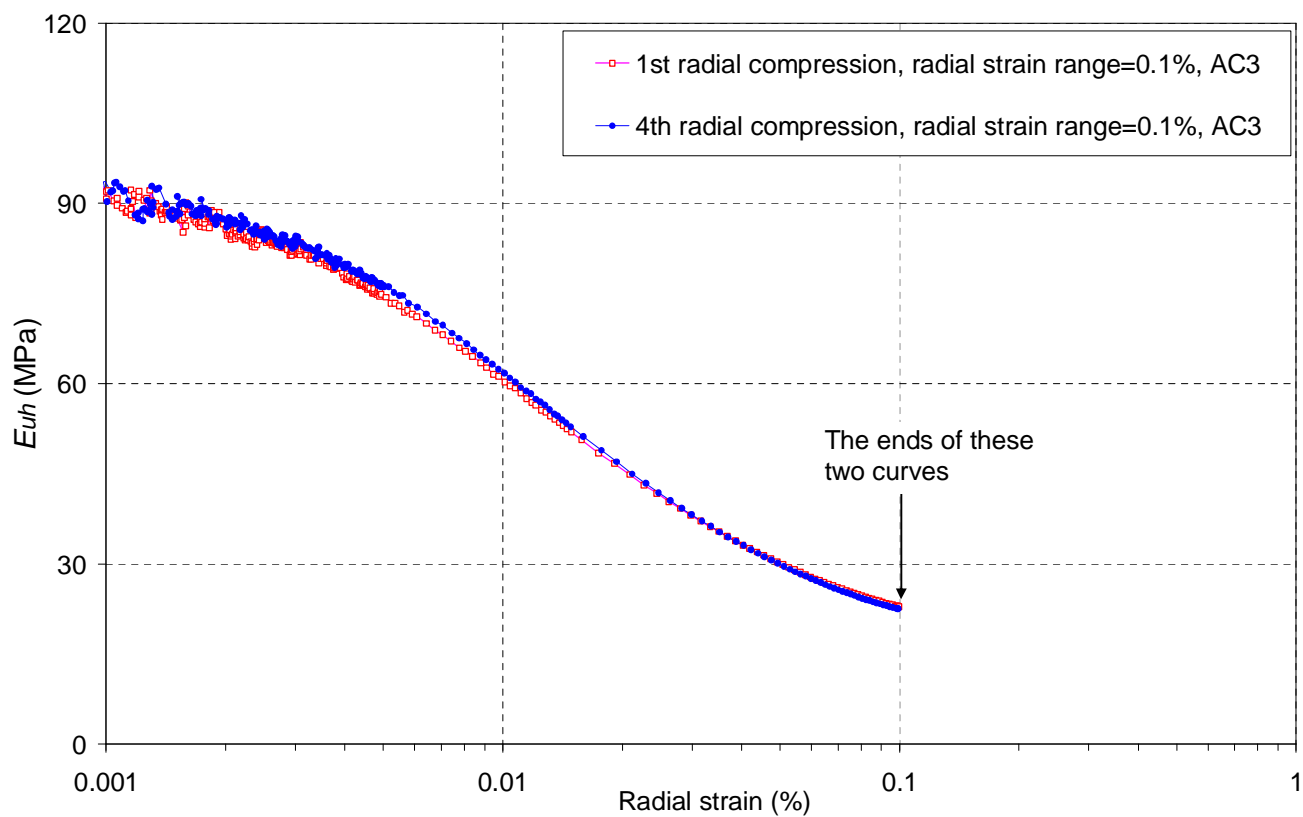
(b) Specimen AC3

Figure 6. Comparison of the secant undrained horizontal Young's modulus (E_{uh}) during the first

and last radial compression under the same undrained cyclic radial strain range
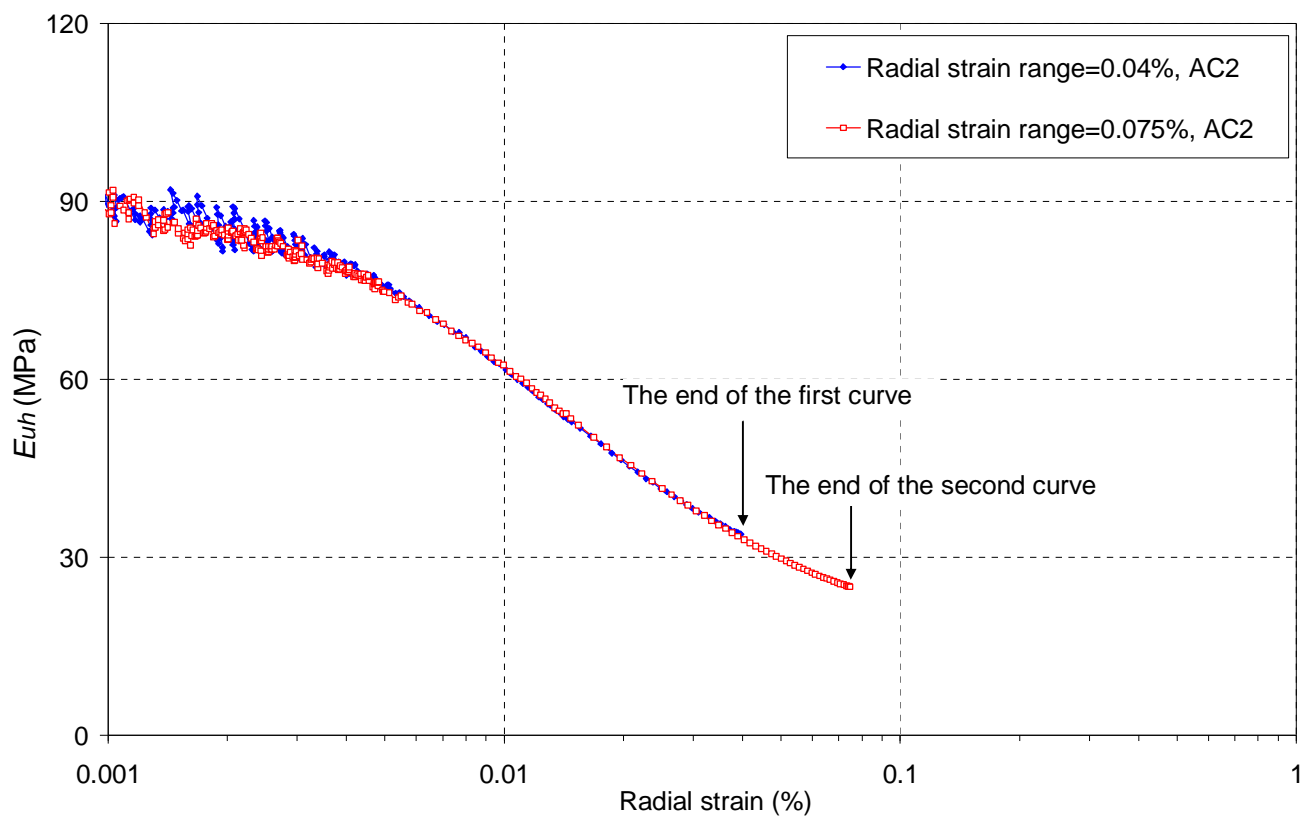
(a) Specimen AC2
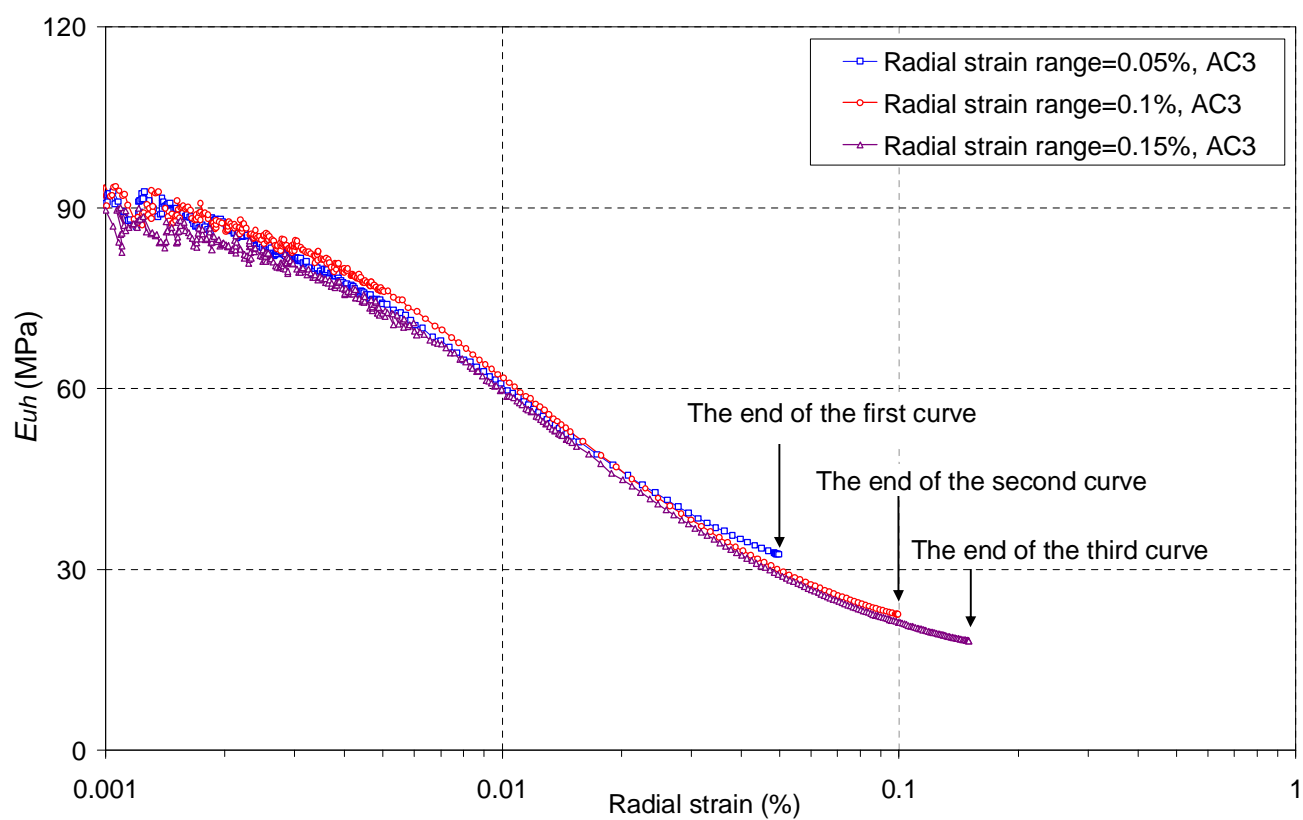
(b) Specimen AC3

Figure 7. Comparison of the secant undrained horizontal Young's modulus (E_{uh}) under different cyclic radial strain ranges
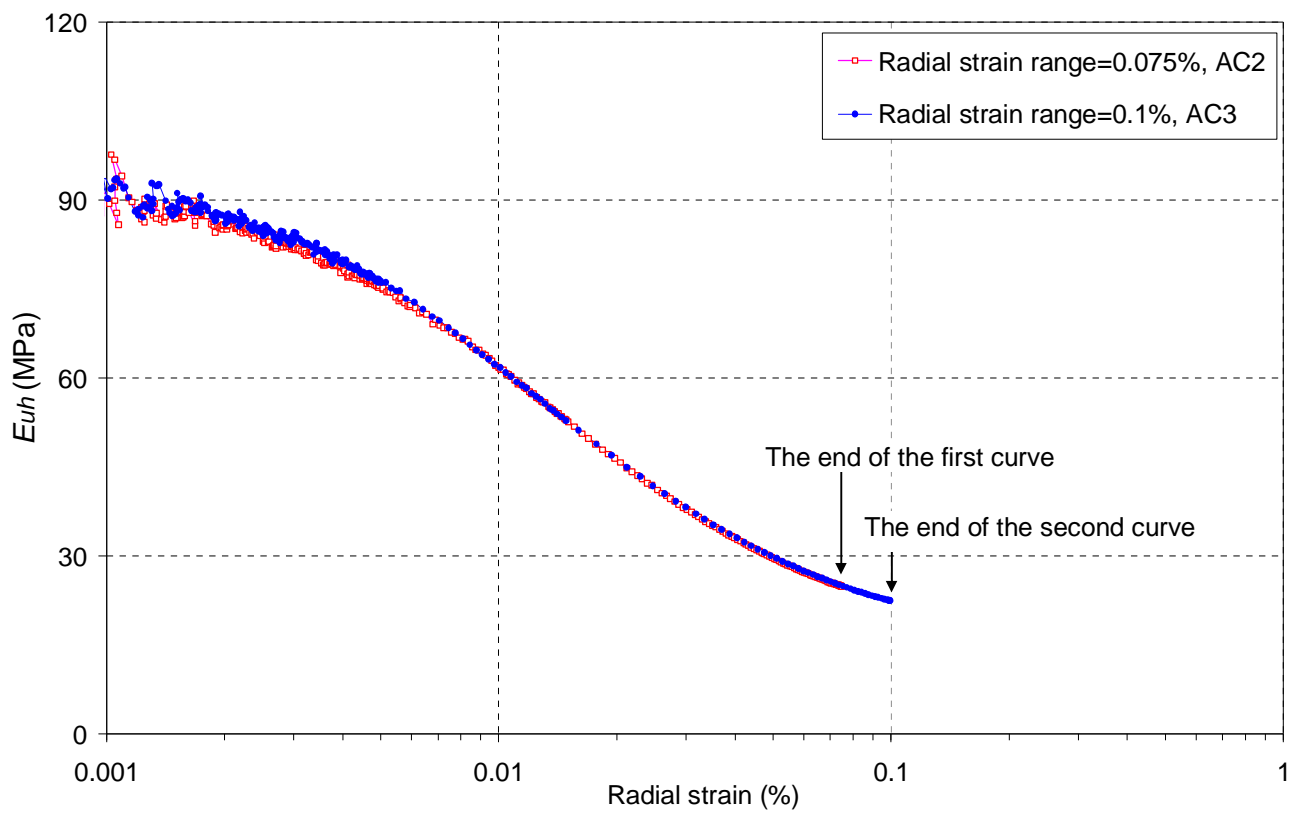
Figure 8. Comparison of typical undrained stiffness behavior of specimens AC2 and AC3
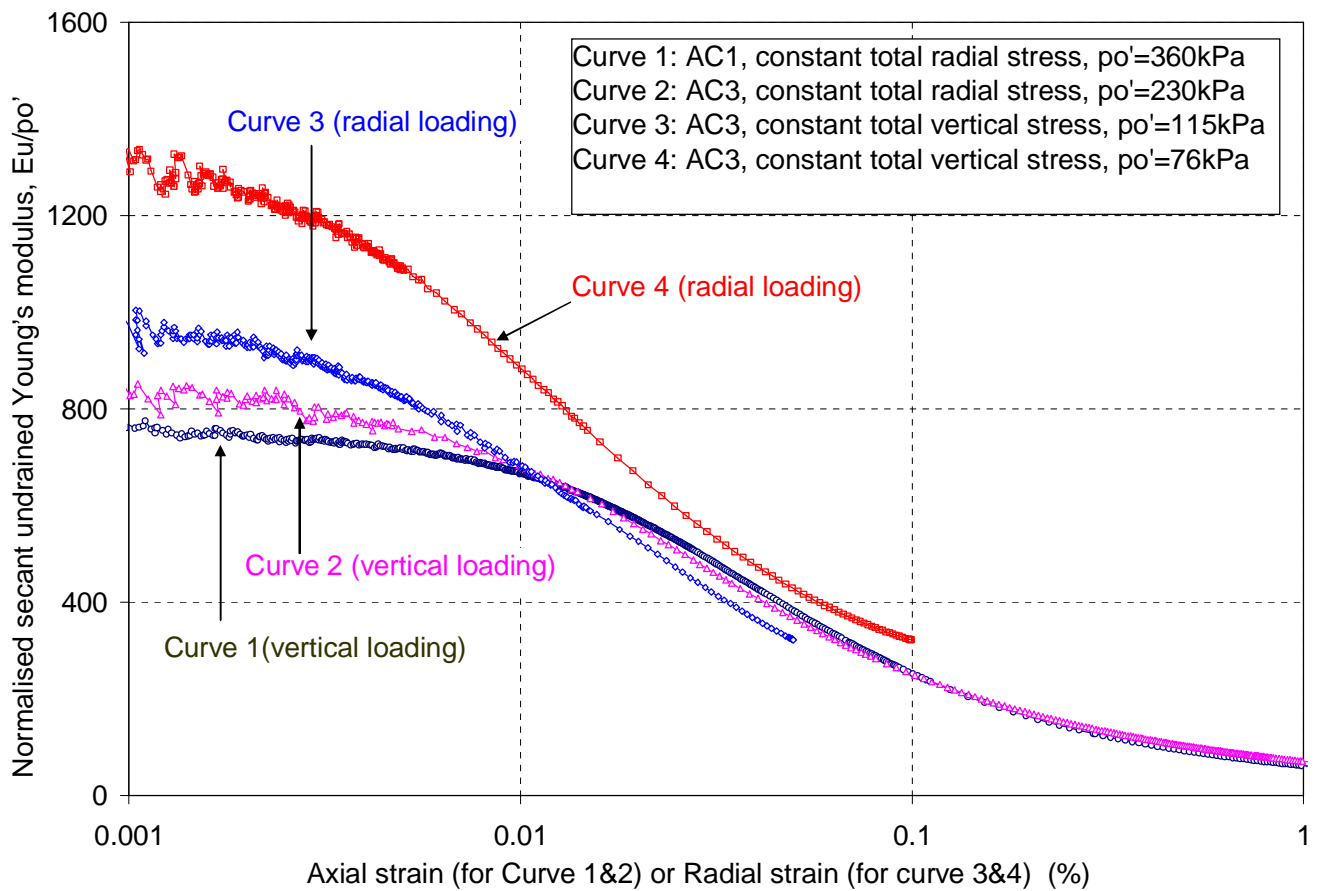
Figure 9. Comparison of normalised horizontal stiffness against radial strain, and

normalised vertical stiffness against axial strain
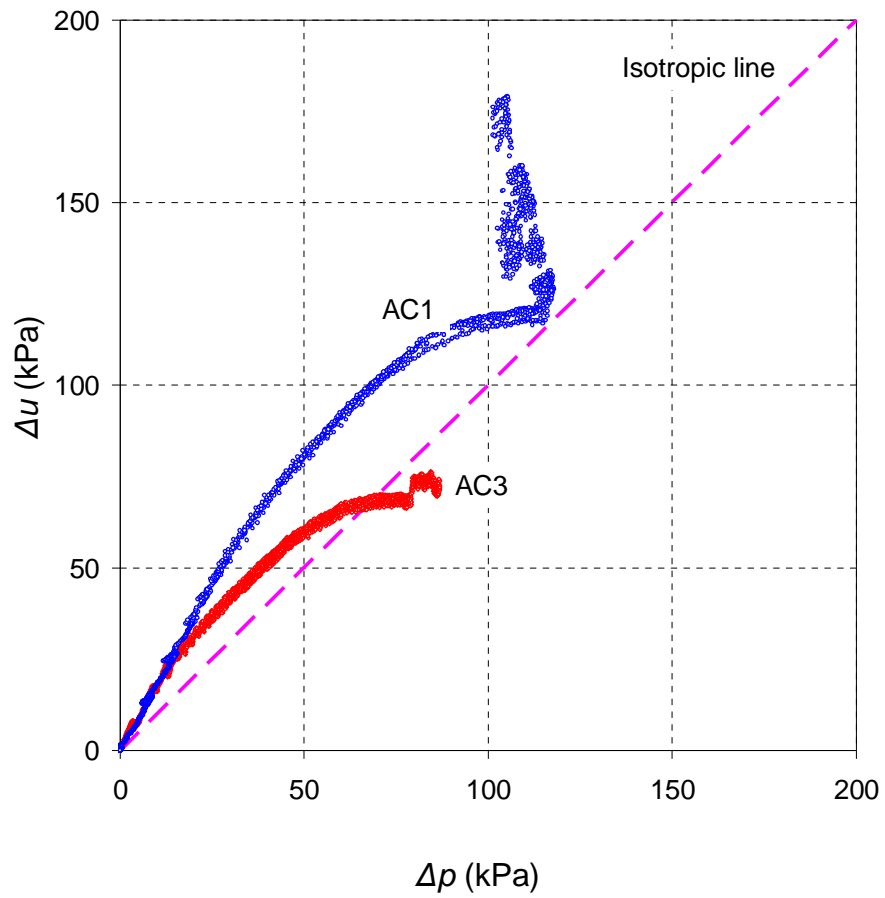
Figure 10. Change in pore water pressure Δu against change in mean total stress Δp during the undrained shearing for AC1 and AC3 with a constant cell pressure
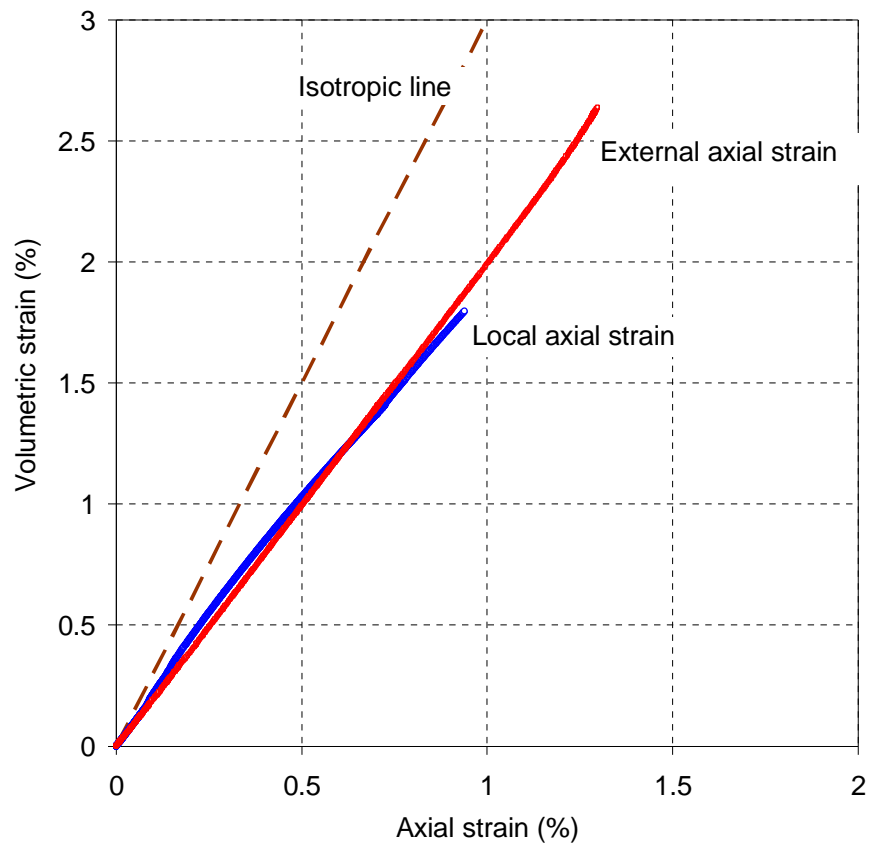
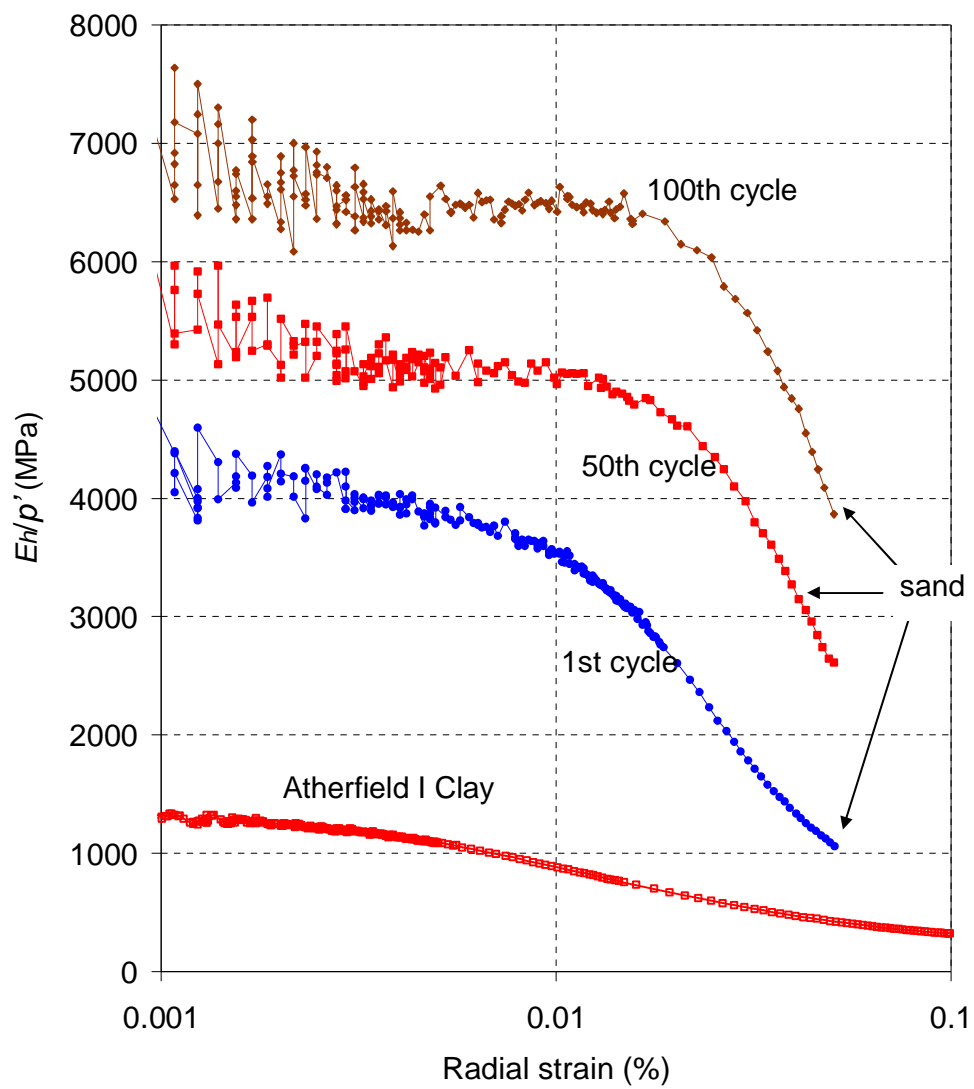Figure 11. Volumetric strain against axial strain for AC3 during isotropic consolidation

Figure 12. Comparison of normalised secant stiffness of Atherfield Clay and loose Leighton Buzzard B sand
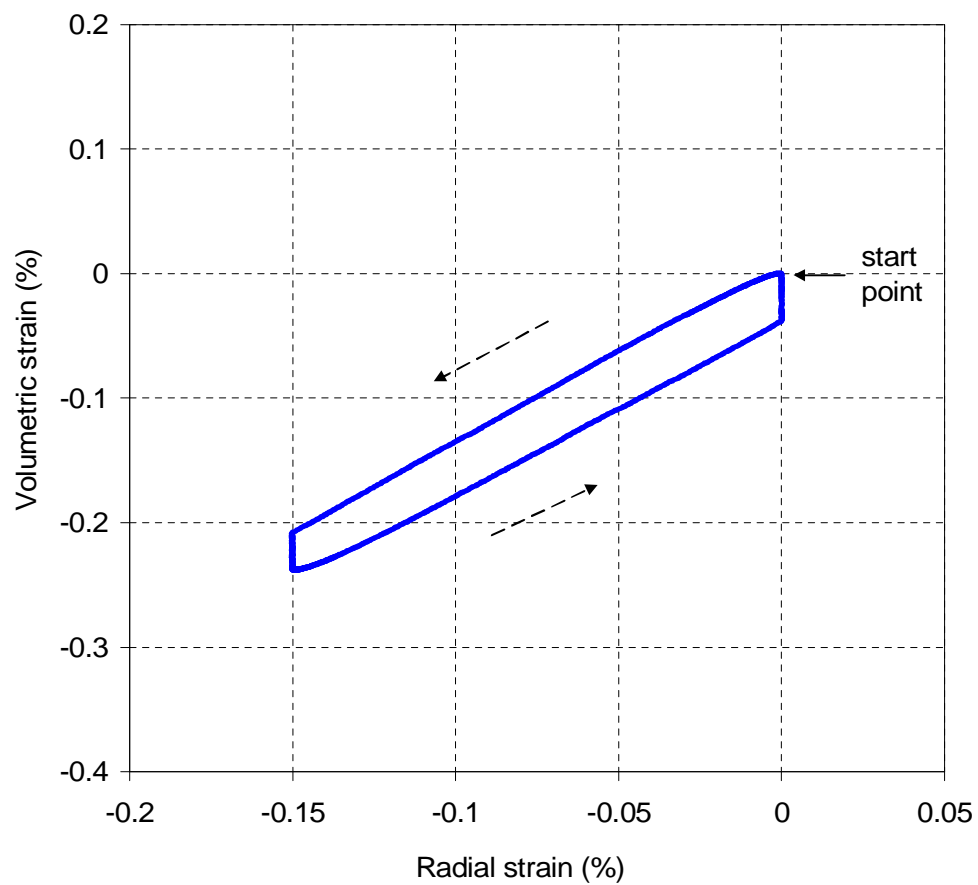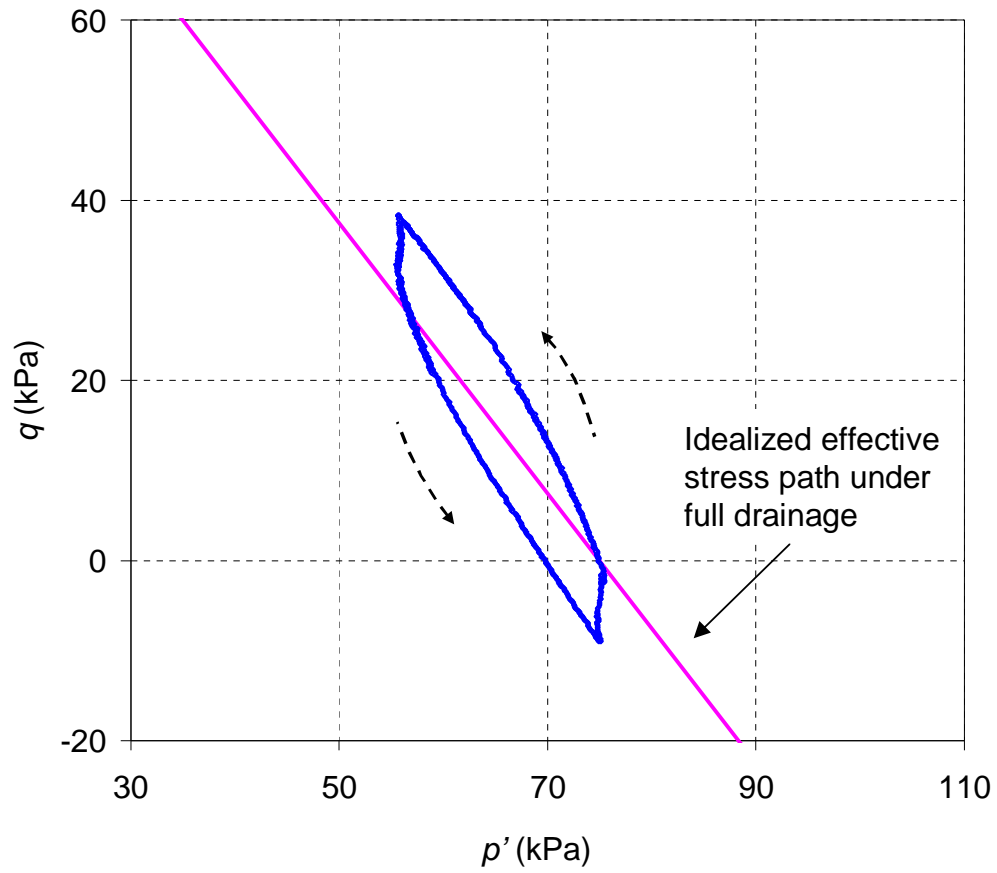
Figure 13. Effective stress path and radial strain-volumetric strain relationship
of AC3 under a drained cyclic radial strain range of 0.15% (1 cycle)